PCCP

ROYAL SOCIETY OF CHEMISTRY

PAPER

View Article Online
View Journal | View Issue



Cite this: *Phys. Chem. Chem. Phys.*, 2022, **24**, 11687

# Thermodynamic study of crown ether–lithium/magnesium complexes based on benz-1,4-dioxane and its homologues†

Iklima Oral, [a] Fanny Ott [a] and Volker Abetz *[ab]

Received 4th March 2022,
Accepted 25th April 2022

DOI: 10.1039/d2cp01076c

rsc.li/pccp

The synthesis and characterization of benz-1,4-dioxane crown ethers (CEs) and some of its homologues are described and analyzed. The effect of added C-atom within the CE ring (increasing the hydrophobicity of the CE ring by increasing the number of $CH_2$-units) on the $Li^+$ and $Mg^{2+}$ complexation within a liquid–liquid extraction (LLE) is investigated and thermodynamically analyzed. The complex stability constant *K*, the change of entropy $\Delta S$ and enthalpy $\Delta H$, and the Gibbs energy $\Delta G$ are determined. The enhanced hydrophobicity of the CE ring results in stronger complexation stability of the $Mg^{2+}$ complex, while the $Li^+$ complexes are less favored. This effect mainly occurs due to the increased entropy term with improved hydrophobicity of the CE. These results indicate a stronger extraction of $Li^+$ in $Mg^{2+}$-containing aqueous resources if more hydrophilic CEs are used.



## 1. Introduction

Crown ethers (CE) are well-known for binding metal cations due to their cyclic cavities and electron donor features.[1] CEs are macrocyclic ligands containing ethyleneoxy units, so-called polyethers. Since the name of these compounds is quickly complicated if larger rings are considered, Pedersen suggested the family name *crown ether*. This definition results from the molecular models and the ability to crown metal cations.[2,3] The general structure of the CE is shown in Fig. 1, where X labels the total number of atoms and Y the total number of heteroatoms within the ring. If the CE arises from an arene catechol compound, the structure is named benzo-X-crown-Y.

The interaction of a CE with a cation is mainly based on the interaction of charge (the metal cation) and dipole (donor atom within the CE ring), which can be influenced by the orientation of the donor atom, cavity size of the CE, type of donor atom (according to the HSAB principle), the substitution of electron-donating and withdrawing compounds and solvent.[4] The large variability of the CE structures and their properties is why they are used in many different applications such as isotope separations,[5] ion determination sensors,[6] phase transfer catalysts,[7] and ion transport through membranes.[8,9]

The application of CEs in solvent extraction is particularly noteworthy since it presents several benefits such as high selectivity, fast extraction rates, and easy application due to simple equipment on a laboratory and industrial scale. Especially in applications with polymers, improved adsorption properties and product recovery are more straightforward.[10–12] The solvent extraction with CEs has been widely used to recover alkali and alkaline-earth metal ions such as $Li^+$, $Na^+$, $K^+$, $Mg^{2+}$, and $Ca^{2+}$.[10,13–16] Different cavity sizes, heteroatoms within the ring such as nitrogen or sulfur, substituents, and complex stoichiometries have been investigated.[17–20] To remove the metal ions from the CE–metal complex, a temperature increase in the system releases the ions from this complex, as shown in the work of Warshawsky and Kahana.[21]

In this work, we synthesized different CEs based on benz-1,4-dioxane by increasing the cavity with an increased alkane chain (increasing the hydrophobicity of the CE). The effect of changing the ring size and increasing hydrophobicity surroundings on metal ion complexation is studied without incorporating other factors such as donor atoms or attached

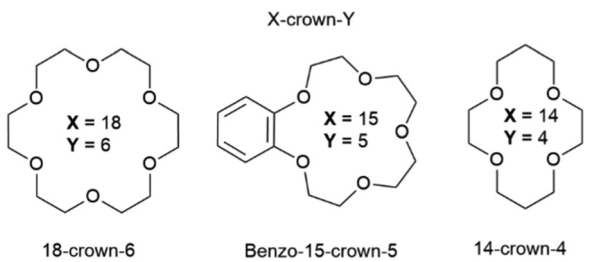


Fig. 1 Illustration of different CE structures.

[a] *Institute of Physical Chemistry, Universität Hamburg, Grindelallee 117, 20146 Hamburg, Germany*
[b] *Helmholtz-Zentrum Hereon, Institute of Membrane Research, Max-Planck-Straße 1, 21502 Geesthacht, Germany. E-mail: volker.abetz@hereon.de*

† Electronic supplementary information (ESI) available. See DOI: https://doi.org/10.1039/d2cp01076c

substituents. In this work, we will focus on the complexation stability of benz-1,4-dioxane-based CEs with the alkali metal ion $Li^+$ and the alkaline-earth metal ion $Mg^{2+}$. In terms of $Li^+$ recovery from brines or seawater, the often-higher $Mg^{2+}$ concentration leads to significant issues due to its similar behavior. Lithium and its compounds are widely used in industrial applications due to their physical and chemical properties and are therefore highly required.[22] Especially in the electric vehicle industry, the demand has increased tremendously. The annual global lithium use was estimated to be 57 700 tons in 2019 and 2020, an 18% increase from 49 100 tons in 2018.[23] Numerous CE adsorbers have been tested for $Li^+$ recovery. For example, the complex stability with benzo-15-crown-5, 12-crown-4, and 14-crown-4 CEs adsorbers have shown excellent complexation properties with $Li^+$; however, complexations with $Mg^{2+}$ and $Na^+$ were also possible.[18,24–32] To selectively extract $Li^+$ from aqueous resources, the complexation behavior of $Li^+$ and the other metal ions is of great importance. Especially the complexation properties of $Li^+$ and $Mg^{2+}$ are of great interest since they have almost the same ion diameter in aqueous solution.[33,34]

In this work the introduced benzo-6-crown-2 (B6C2), benzo-7-crown-2 (B7C2), and benzo-8-crown-2 (B8C2) structures (Fig. 2) are investigated regarding metal ion complex stability since, as far as we know, such adsorbers have not yet been studied. Moreover, the influence of the hydrophobic environment within the ring on the respective ions will be tested and discussed. The thermodynamic properties of $Li^+$ and $Mg^{2+}$ complexes will be further investigated by determining the enthalpy and entropy change during the complexation process.

## 2. Results and discussion

### 2.1. Synthesis of benz-1,4-dioxane crown ethers and homologues

One of the most widely used methods for the syntheses of CEs is the Williamson ether synthesis, which was introduced by Alexander William Williamson.[35] The Williamson ether synthesis is a variant of the nucleophilic substitution second-order reaction ($S_N2$), characterized by a transition state. An alcohol, here: catechol **1**, is converted into an dialcoholate **2** with the aid of a non-nucleophilic base $K_2CO_3$ (Fig. 3).[36] It is worth mentioning that the alkoxides exhibit a higher nucleophilicity than alcohols, due to their increased electron density at the partially negatively charged oxygen atom, which accelerates the speed of the reaction. Due to their high base strength, ether synthesis is limited to the use of primary alkyl halides, since otherwise

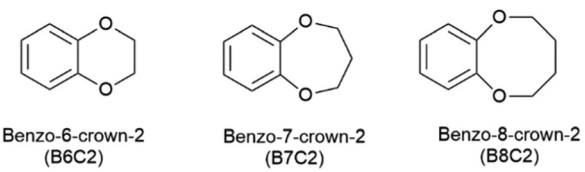


Fig. 2 Benz-1,4-dioxane-based CEs with an increased alkali chain.

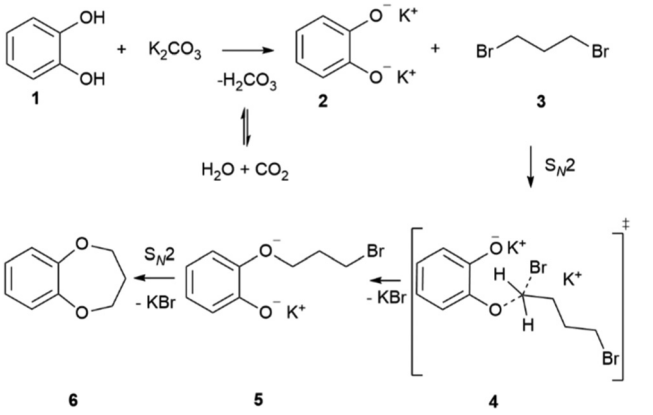


Fig. 3 Illustration of the reaction mechanism of dipotassium catecholate with 1,3-dibromopropane under $S_N2$ conditions to synthesize B7C2.

side-reactions would occur from the competing bimolecular elimination reaction (E2). It is worth mentioning that the use of phenoxides principally can lead to another side reaction, the *C*-alkylation. However, this can be prevented by using inert solvents such as benzene, toluene, xylene or polar aprotic solvents such as dimethylformamide (DMF) and dimethylsulfoxide (DMSO) to favor the oxygen alkylation.[36] In the next step, the dialcoholate **2** reacts with a primary dihalogenide **3** (here: 1,3-dibromopropane) *via* a concerted, five-membered transition state **4** to form a new ether bond. An alkyl dibromide was chosen as an alkyl dihalide since the leaving capacity of the leaving group correlates with its ability to stabilize the negative charge and increases within the group F < Cl < Br < I due to increasing polarization capacity. In a further $S_N2$ reaction, the oxygen nucleophile intramolecularly attacks the electrophilic center of the C–Br bond **5** and forms the seven-membered B7C2 CE ring **6** with two oxygen donor atoms. The synthesis of B8C2 follows the same reaction mechanism. For this, 1,4-dibromobutane was used as an alkyl dihalogenide. The synthetic routes were adapted/modified from the work of Y.-F. Ji *et al.*[37] and H.-L. Zhu.[38] Since these CEs have not been previously considered as ligands, sufficient analysis of these structures is performed by nuclear magnetic resonance (NMR) spectroscopy (Fig. 4) and infrared (IR) spectroscopy (Fig. S3 and S7, ESI†), differential scanning calorimetry (DSC) measurements (Fig. S4 and S8, ESI†), and mass spectrometry (MS) (Fig. 5). The $^1$H NMR data before purification of the products and the $^{13}$C NMR spectra are also documented in the ESI.† The data of the $^1$H- and $^{13}$C spectra are in good agreement with the data from the literature. To the best of our knowledge, the gas chromatography-MS (GC-MS), IR spectroscopy, and DSC data of these compounds have not been reported before.

The molecular ion peak found at 151 000 *m*/*z* agrees with the calculated molecular weight for approximately B7C2 ($M$ = 151.178 g mol$^{-1}$). The main fragmentation reactions consist of a benzyl cleavage. The delocalized π-electron system of the aromatic compound favors the formation of a stable benzyl ion (80 000 *m*/*z*). The possible minor cleavage product is 1,3-cyclobutadiene (52 000 *m*/*z*), formed by re-ionization. The peak

 

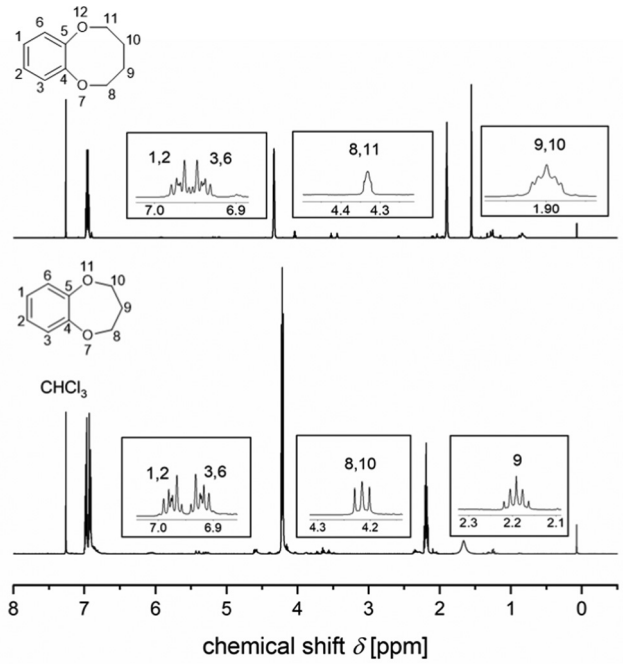


Fig. 4 $^{1}$H NMR spectrum of the B7C2 (bottom) and B8C2 (top). The spectrum was recorded in $CDCl_3$ and shows the significant signals and their multiplicities on larger scale.

at 121 000 *m*/*z* shows a fragmentation based on a benzyl cleavage and hydrogen rearrangement, followed by McLafferty rearrangement and fragmentation. Instead of the McLafferty rearrangement, direct fragmentation of the radical cation is possible, whose quinoid cleavage product leads to the peak at 109 000 *m*/*z*. The GC-MS spectrum of the B8C2 shows a molecular ion peak at 164 000 *m*/*z*, which is in good agreement with the calculated molecular weight of $M$ = 164 080 *m*/*z*. The cleavage product of the McLafferty rearrangement at 121 000 *m*/*z* has a lower intensity than B7C2. Thus, it can be assumed that the formation of this molecule ion peak decreases with the increasing ring size of the CE, which is most likely due to the steric relief caused by the chain breakage.

### 2.2. Pre-extraction experiments

In the following, the extraction properties of the newly synthesized B8C2 and B7C2 CEs and B6C2 (commercially available) with $Li^+$ and $Mg^{2+}$ in a liquid-liquid extraction (LLE) are investigated and the effect of ring size and hydrophobicity environment of the ring are discussed. To ensure that the CEs remain in the organic phase during the LLE, blank tests were performed. For this purpose, the CE was dissolved in an organic phase (here: DCM) and LiCl in the aqueous phase. The two-phase mixture was shaken vigorously, and the aqueous phase was subsequently analyzed by UV-vis spectroscopy. Since LiCl shows no absorption in the UV-vis spectrum, any visible signal should refer to the CE. Fig. S13 (ESI†) clearly shows that no absorption maximum is observed in the aqueous phase after extraction for the B7C2 and B8C2 CE structures. The B6C2 shows a small signal (black curve) below 1% and thus one can conclude that the CE–cation complex remains mainly in the organic phase.

### 2.3. Determination of the thermodynamic complex constant *K*

The extractability of the metal salts by B6C2, B7C2, and B8C2 was investigated using a reference series of the respective cation. To determine the complexing properties of the CEs, the complex constant $K$ was determined. To ensure UV-vis spectroscopic evaluation of salt complexation, counterions were used that allow π–π* excitation in the ultraviolet to visible spectral range through conjugated double bond systems and (anti-)auxochromic groups. The chosen metal salt dyes and their corresponding UV-vis spectrum can be found in the ESI† (Fig. S9–S12).

For the LLE of the CE and cation dye, a molar ratio of CE to metal ion ranging from 25 : 1 to 11 : 1 was used. The reaction can be described as shown in eqn (1).

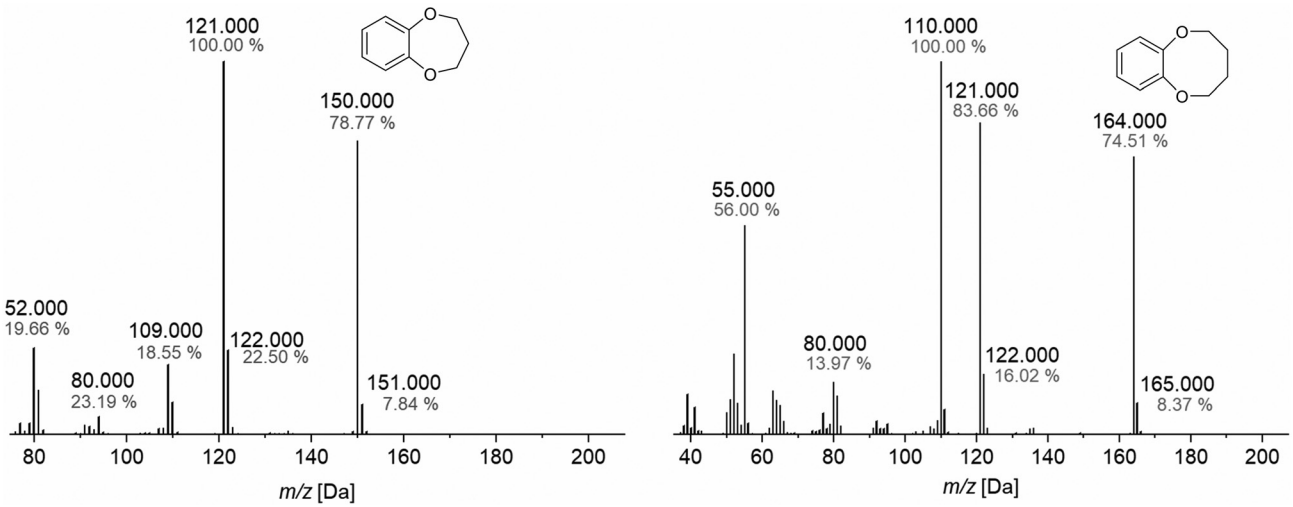


Fig. 5 GCMS spectrometry of B7C2 (left) and B8C2 (right).

$$m\mathrm{M}^{z+}x\mathrm{X}^{v-}_{(\mathrm{aq})} + n\mathrm{CE}_{(\mathrm{org})} \rightarrow (\mathrm{M}_m\mathrm{CE}_n)^{mz+}\mathrm{X}^{xv-}_{x(\mathrm{org})} \quad (1)$$

where $m$ and $x$ are the stoichiometric factors of the cation M of charge $z_+$, and the corresponding counterion X of charge $v_-$, and $n$ as the equivalents of the CE obligatory for complexation. For all cations $m = 1$ applies, while $x = 1$ applies for $Li^+$ and $x = 2$ applies for $Mg^{2+}$. A calibration curve of each salt solution was performed before extraction to determine the concentration in the aqueous phase using the Lambert–Beer law. The calibration was performed shortly before the measurement series and conducted using the same stock solution as the extraction experiments to guarantee the most precise data. The complex constant $K$ of the extraction process was calculated according to the law of mass (eqn (2)):[10,39]

$$K = \frac{\left[(\mathrm{M}_m\mathrm{CE}_n)^{mz+}X^{xv}_{x(\mathrm{org})}\right]}{(Q\cdot(\gamma_+[\mathrm{M}^{z+}]^m)\cdot(\gamma_-[\mathrm{X}^{v-}]^x))\cdot[\mathrm{CE}]^n} \quad (2)$$

with the mean activity coefficients $\gamma_\pm$ and the stoichiometric coefficient $Q$. Due to the electroneutrality condition, only the activity of the entire system can be determined. Therefore, the mean activity coefficient $\gamma_\pm$ is applied for $\gamma_-$ and $\gamma_+$, which can be calculated according to the Debye–Hückel-equation (see eqn (3)).

$$\log(\gamma_\pm) = -A\cdot|z_+v_-|\cdot\sqrt{I_\mathrm{a}} \quad (3)$$

$I_\mathrm{a}$ is the ionic strength and $A$ is a dimensionless factor, which has a value of 0.509 at 25 °C.[40] The ionic strength $I_\mathrm{a}$ can be calculated according to eqn (4):

$$I_\mathrm{a} = \frac{1}{2}\sum_i c_i\cdot z_i^2 \quad (4)$$

With $c_i$, the molar concentration of the ion (mol $L^{-1}$) and $z_i$ the charge number of the ions. The stoichiometric coefficient $Q$ can be calculated according to eqn (5).

$$Q = (m^m\cdot x^x)^{\frac{1}{m+x}} \quad (5)$$

### 2.4. Extraction studies of B6C2, B7C2 and B8C2 with $Li^+$ and $Mg^{2+}$

In the following, the complex stability of B6C2, B7C2, and B8C2 at different concentrations with $Li^+$ and $Mg^{2+}$ at 25 °C is determined. The complexation constant $K$ was calculated for a single and a sandwich-type cation–CE complexation. An illustration of the newly formed structure is exemplarily presented in Fig. 6 for the B7C2 with $Li^+$ and $Mg^{2+}$ and the corresponding anions. Since $Li^+$ and $Mg^{2+}$ are preferentially complexed in coordination number (CN) 4,[41,42] a sandwich complex can be assumed (two CE ligands crown one metal ion). Furthermore, the cavity size of the CE might be too small for the metal ions to fit into the CE cavity.[34] Therefore, the data presented here are calculated based on the assumption of a sandwich-type complexation.

In the complexation process of metal ions from aqueous solutions, the formation of the hydration shell plays an essential role.

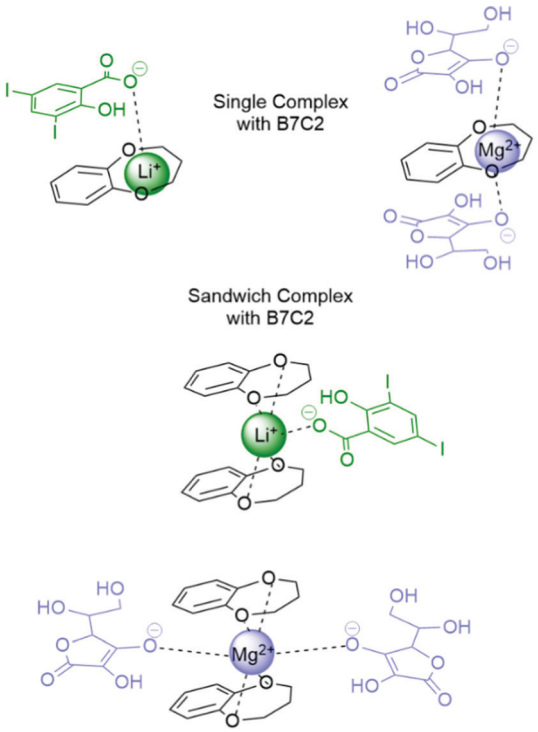


Fig. 6 Schematic illustration of the B7C2–Li and Mg single and sandwich-type complex with corresponding anions.

The hydration shell must first be removed from metal ions to be complexed. The strength of the hydration shell depends on the charge and the size of the metal ion. The energy freed when one mole of ions undergoes hydration is called the hydration enthalpy $\Delta H_\mathrm{hyd}$, which is the highest for $Mg^{2+}$ (−1922 kJ $mol^{-1}$), followed by $Li^+$ (−521 kJ $mol^{-1}$).[43] The evaluated complex stability constants $K$ for the molar ratio of CE to metal ion ranging from 25 : 1 to 11 : 1 for single and sandwich-type complexation can be found in Fig. S14 and Table S1 (ESI†). A graphical illustration of the complexation constants $K$ of the respective complexes is shown in Fig. 7 (values refer to the more likely sandwich-type complexation). It is already known that the substitution of the oxygen donor atoms with less electronegative atoms such as nitrogen favors the complexation of $Mg^{2+}$ (as expected according to the HSAB principle). However, the influence of a more hydrophobic environment with a simple alkyl chain has not been studied yet. The introduction of a more hydrophobic ring shows a stronger complex stability constant $K$ for $Mg^{2+}$ which is indicated by the following trend B8C2 = B7C2 > B6C2. For $Li^+$, on the other hand, the trend is *vice versa* showing an increased $\log K$ in the following trend: B6C2 ≈ B7C2 > B8C2 and thus decreasing with higher hydrophobicity of the ring. According to the HSAB principle $Li^+$ (hardness $\eta$ = 35.12) is a harder base than $Mg^{2+}$ ($\eta$ = 32.55),[44,45] which could explain the obtained trend.

### 2.5. Temperature-dependent extraction studies of B6C2, B7C2 and B8C2 with $Li^+$ and $Mg^{2+}$

In the following, enthalpic and entropic values are determined experimentally by temperature-dependent LLE to clarify the differences of complex stability for the B6C2, B7C2 and B8C2

 

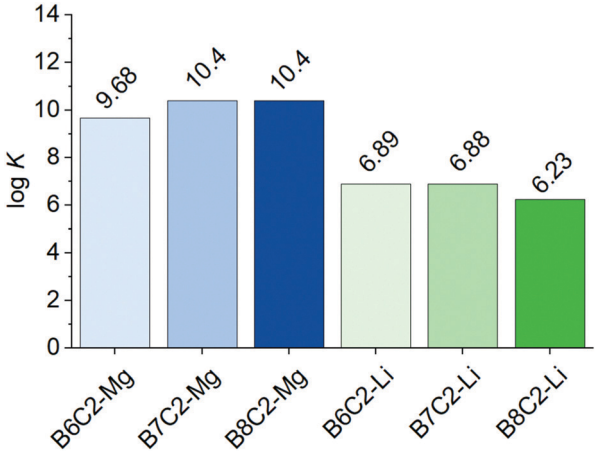


Fig. 7 log $K$ of the CE : metal ion complexes with B6C2, B7C2, and B8C2 with $Mg^{2+}$ and $Li^{+}$ at a constant molar ratio of CE : metal ion of 14 : 1.

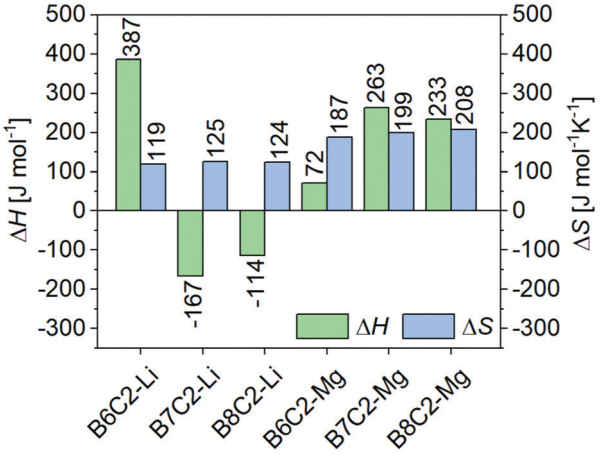


Fig. 8 Enthalpy and entropy changes after complexation of the CE with the metal ions $Li^{+}$ and $Mg^{2+}$ at a constant molar ratio of CE : metal ion of 14 : 1. The green bars represent the change in enthalpy $\Delta H$ after extraction and the blue bars the change in entropy $\Delta S$, respectively.

CEs more precisely. The relation between the complex constant $K$ and temperature is described by the Van't Hoff equation (VH, eqn (6)) assuming that $\Delta H$ and $\Delta S$ are temperature independent.

$$\ln K = -\frac{\Delta H}{R} \cdot \left(\frac{1}{T}\right) + \frac{\Delta S}{R} \quad (6)$$

The VH equation arises from the combination of the Gibbs energy of reaction and the Gibbs energy isotherm equation, which is described in eqn (7) and (8). $R$ labels the molar gas constant (8.314 J $mol^{-1}$ $K^{-1}$).

$$\Delta G = \Delta H - T\Delta S \quad (7)$$

$$\Delta G = -RT \ln K \quad (8)$$

The so-called VH plot results from eqn (6). The natural logarithm $\ln K$ is a linear function of the reciprocal temperature $1/T$. The plot of the values results in a linear regression, where the slope gives $-\frac{\Delta H}{R}$ and the intercept $\frac{\Delta S}{R}$. The VH plots are shown in Fig. S15 (ESI†) and the corresponding values to determine $\Delta S$ and $\Delta H$ can be found in Table S2 (ESI†). The data of the enthalpy and entropy changes $\Delta H$ and $\Delta S$ after complexation of B6C2, B7C2, and B8C2 with $Li^{+}$ and $Mg^{2+}$ are shown in Fig. 8. The green bar labels $\Delta H$ and the blue bar labels $\Delta S$.

Generally, an enthalpy gain occurs if new interactions proceed between the metal ion and the donor atoms of the CE. On the other hand, the anion interacts less pronounced in the organic phase compared to the aqueous phase, resulting in an enthalpy loss.[39] The enthalpy change $\Delta H$ is highest for the B6C2 for $Li^{+}$ and decreases rapidly when the ring size as well as the hydrophobicity increases. In fact, negative values are obtained for the B7C2 and B8C2 CEs, which might be due to the weaker $\Delta H_{hyd}$ of $Li^{+}$ compared to $Mg^{2+}$, making the desolvation less energy-consuming and, therefore, enthalpic change more favorable. However, this is not the case for B6C2–Li. The energy contributions are significantly higher for the $Mg^{2+}$ complexes, which is most likely due to the stronger bonding of the water molecules to the $Mg^{2+}$ in the aqueous phase. In addition, two anions have to be freed from the hydration shell compared to the Li complex to form the CE–Mg complex (compare with Fig. 6). In addition, $\Delta H$ increases for the more hydrophobic CE rings such as B7C2 and B8C2 in comparison to B6C2.

The change of Gibbs energy of a system is an interplay between $\Delta H$ and $\Delta S$. The change of entropy $\Delta S$ is almost identical for $Li^{+}$ complexes and increases only slightly with increasing hydrophobicity of the CE. On the other hand, $\Delta S$ increases with growing hydrophobicity for the CE–Mg complexes, which is most likely the reason for the higher complex stability $K$ (Fig. 7). The higher $\Delta S$ of $Mg^{2+}$ complexes compared to $Li^{+}$ ones most-probably result from the released water molecules, which were strongly bound to the $Mg^{2+}$ ion before complexation. As previously mentioned, the hydration enthalpy $\Delta H_{hyd}$ is almost four times larger than the enthalpy that would be required to desolvate lithium. Accordingly, the water molecules are much more strongly bound to the $Mg^{2+}$. In addition, in the case of the $Mg^{2+}$ complexes, two anions are attached to the complex so that twice the amount of water molecules are released. In contrast, the formation of complexes in the organic phase also leads to entropy loss since the CEs lose mobility. The larger the complex, the greater this loss. The entropy loss is thus more significant for a sandwich-type complex compared to a single complex. The change in entropy $\Delta S$ is, therefore an interplay between the gain in entropy due to the release of water molecules in the aqueous phase and the loss of entropy due to the binding of the ligands and anions to the metal ion in the organic phase.

To describe the energy of a system and its voluntariness of the complex formation, the Gibbs energy $\Delta G$ is used. Fig. 9 shows the calculated $\Delta G$ values calculated according to eqn (7) by performing extraction at room temperature (grey bar) and by eqn (8) conducting temperature-dependent extractions using the VH equation ($\Delta G$ (VH), orange bar). Both $\Delta G$ values agree well with each other. All reactions are exergonic and proceed

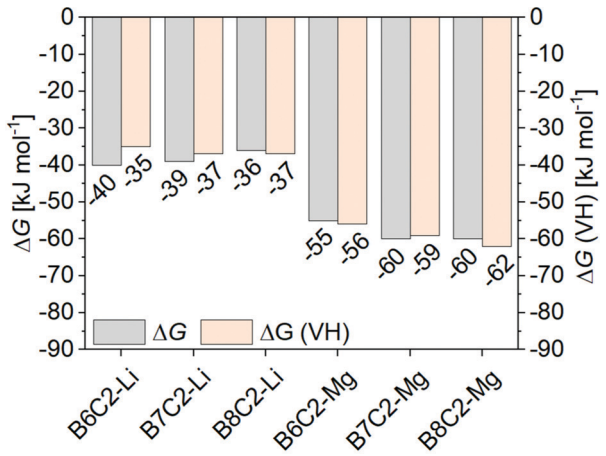


Fig. 9 Gibbs energy calculated by the Gibbs–Helmholtz equation ($\Delta G$), grew bars and from the Gibbs energy isotherm equation based on the Van't Hoff plot ($\Delta G$ (VH), orange bars at a constant molar ratio of CE : metal ion of 14 : 1). The data represent the values for $T$ = 25 °C.

voluntarily, with the $Mg^{2+}$ complexes being more favorable. This effect is more pronounced with increasing hydrophobicity of the CE ring.

The CEs prepared in this work are new adsorbers for lithium isolation that have not been previously considered in the group of benz-1,4-dioxane homologues with an increasing alkane chain. In addition, CE B7C2 in particular is less expensive in comparison to the commercially available 12-crown-4 and 15-crown-4 CEs that are commonly used for lithium isolation and since it is less soluble in water, the yield of complexed lithium is larger.

# 3. Conclusions

B7C2 and B8C2 CEs were synthesized and compared with B6C2 in LLE to investigate the $Li^+$ and $Mg^{2+}$ extractability from aqueous solution. Thermodynamic parameters such as the complex stability constant $K$, the Gibbs energy $\Delta G$ (calculated from room temperature and temperature-dependent extractions), and the change in entropy $\Delta S$ and enthalpy $\Delta H$ were determined and discussed. The increase of the number of C atoms within the CE ring (higher hydrophobicity) leads to higher $Mg^{2+}$ complex stability, while the $Li^+$ complex stability is decreased. The higher stability of $Mg^{2+}$ complexes is most likely based on a greater change in change of entropy $\Delta S$ with increasing hydrophobicity. In summary, the data reported here show that the effect of hydrophobicity has brought us much closer to the selective extraction of $Li^+$ over $Mg^{2+}$ and that these results can further narrow the choice of future adsorbents for lithium extraction to find a suitable material.

# 4. Experimental

## 4.1 Materials

1,4-Benzdioxane (98%, Sigma-Aldrich, Schnelldorf, Germany), (+)-Mg-(L)-ascorbate (98%, Sigma-Aldrich, Schnelldorf, Germany), lithium 3,5-diiodosalicylate (>99%, LIS, Sigma-Aldrich, Schnelldorf, Germany), potassium carbonate (99%, Sigma-Aldrich, Schnelldorf, Germany), catechol (99%, Sigma-Aldrich, Schnelldorf, Germany), dichloromethane (DCM) (>99%, Acros, Schwerte, Germany), petrol ether (technical grade), ethyl acetate (technical grade), 1,3-dibromopropane (>99%, Sigma-Aldrich, Schnelldorf, Germany), 1,4-dibromobutane (>99%, Sigma-Aldrich, Schnelldorf, Germany), 2-propanol (>99%, Sigma-Aldrich, Schnelldorf, Germany) *n*-hexane (95%, VWR Chemicals, Darmstadt, Germany), chloroform-$d_1$ (>99%, EurisoTop, Saarbrücken, Germany) were used as received without further purification unless noted otherwise. Deionized water was purified with a Milli-Q® integral water purification system.

## 4.2 Methods

**Fourier transform infrared spectroscopy (FTIR).** The ATR-FTIR spectra were taken on powders of ground dry interpenetrating network gel samples with a Bruker IFS 66V/S FTIR, with a wide-band Mercury Cadmium Telluride (MCT) detector, KBr mid-IR beam splitter, and Pike diamond-ATR module. Each spectrum was averaged over 64 scans at a resolution of 2 $cm^{-1}$.

**Nuclear resonance spectroscopy (NMR).** $^1H$ NMR and $^{13}C$ NMR spectra were recorded at ambient temperature using a 500 MHz Bruker AVANCE II spectrometer in $CDCl_3$. The residual signals at $\delta$ = 7.26 for $CDCl_3$ were used as an internal standard for the chemical shifts.

**UV/Vis spectroscopy.** The UV-Vis spectra were recorded with a spectrophotometer UV5 from METTLER TOLEDO at room temperature using a scan time of 10 s.

**Gas chromatography (GC) with mass spectrometry (MS) coupling.** The measurements were carried out in a Thermo ISQ LT EI coupled to a Thermo Trace 1300.

**Differential scanning calorimetry.** DSC measurements were conducted on a DSC 204 F1 Phoenix from Netzsch. The experiments were run with a scanning rate of 10 K $min^{-1}$ at different temperature ranges and conducted under an inert nitrogen atmosphere. A sample between 5–10 mg was weighed into a 40 μL aluminum crucible which was capped afterward using a pierced lid. The data processing was performed by the Netzsch software Protheus analysis.

## 4.3 Synthetic procedures

In this work, the preparation of the crown ethers was carried out in a modified form according to a prescription of Huang *et al.*[37] The reactions took place under a nitrogen atmosphere.

**Synthesis of benzo-7-crown-2**

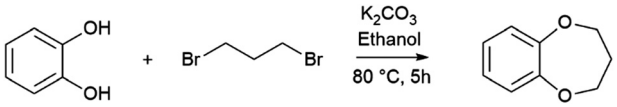


Catechol (5.6 g, 51 mmol, 1.0 eq.), 1,3-dibromopropane (14 g, 7.1 mL, 69 mmol, 1.4 eq.) and potassium carbonate (25 g, 0.18 mol, 3.5 eq.) were dissolved in ethanol (27% (v/v), 150 mL). The green mixture was heated under reflux for 5 h at 80 °C and turned into an orange mixture. The reaction was cooled to room

 

temperature and filtrated under reduced pressure. The crude product was purified two times with column chromatography on silica gel with a mobile phase of petrol ether and ethyl acetate (30 : 1 v/v) and (25 : 1 v/v). The product was obtained as a colorless oil (4.1 g, 54%). $^1$H NMR (500 MHz, $CDCl_3$, 25 °C): $\delta$ [ppm] = 7.00–6.91 (m, Ar-H, 4H), 4.22 (t, $^3J$ (H, H) = 3 Hz, O–$CH_2$, 4H), 2.19 (quint., $^3J$ (H,H) = 3 Hz, –$CH_2$, 2H); $^{13}$C NMR (500 MHz, $CDCl_3$, 25 °C): $\delta$ [ppm] = 152 ($C_4$), 124 ($C_4$–CH–**C**H), 122 ($C_4$–**C**H–CH), 70.9 (O–**C**$H_2$–), 32.2 (–**C**$H_2$); GC-MS (EI): *m*/*z* (%): $[M]^+$ calcd for $C_9H_{10}O_2^+$: 151.08, found 151.00 (8) $[M^+]$, 121.00 (100) $[C_7H_7O_2^+]$, 109.00 (19) $[C_6H_4O_2^+]$, 80.00 (23) $[C_6H_6^+]$, 51.02 (20) $[C_4H_3^+]$; IR (KBr): $\tilde{\nu}$ [$cm^{-1}$] = 3037 (w), 2950 (m), 2866 (w), 1580 (m), 1490 (s), 1246 (s), 1048 (s), 751 (s).

**Synthesis of benzo-8-crown-2**

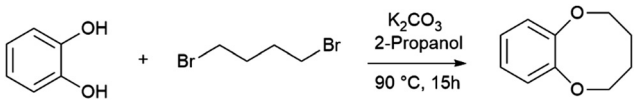


Catechol (6.7 g, 61 mmol, 1.0 eq.) was dissolved in 2-propanol (14% (v/v), 170 mL). After adding potassium carbonate (29.5 g, 214 mmol, 3.5 eq.), 1,4-dibromobutane (7.65 mL, 14 g, 64 mmol, 1.0 eq.) was added dropwise to the reaction mixture. The turbid reaction mixture was heated under reflux for 15 h at 90 °C. The red solution was cooled to room temperature and subsequently extracted 5 times with dichloromethane. The eluate was washed with water and brine. Any residue of solvent was removed under reduced pressure. The orange residue was purified two times with column chromatography on silica gel with a mobile phase of *n*-hexane and ethyl acetate (8 : 1 v/v) and (10 : 1 v/v). The product was obtained as a light-yellow-colored oil (0.3 g, 3%). $^1$H NMR (500 MHz, $CDCl_3$, 25 °C): $\delta$ [ppm] = 6.98–6.93 (m, Ar-H, 4H), 4.34–4.32 (m, O–$CH_2$, 4H), 1.91–1.89 (m, –$CH_2$, 4H); $^{13}$C NMR (500 MHz, $CDCl_3$, 25 °C): $\delta$ [ppm] = 150 ($C_4$), 124 ($C_4$–CH–**C**H), 123 ($C_4$–**C**H–CH), 72.8 (O–**C**$H_2$–), 27.1 (–**C**$H_2$); GC-MS (EI): *m*/*z* (%): $[M]^+$ calcd for $C_{10}H_{12}O_2^+$: 165.09, found 165.00 (8) $[M^+]$, 121.00 (84) $[C_7H_7O_2^+]$, 110.00 (100) $[C_6H_4O_2^+]$, 80.00 (14) $[C_6H_6^+]$, 55.00 (56) $[C_4H_3^+]$; IR (KBr): $\tilde{\nu}$ [$cm^{-1}$] = 3069 (w), 2931 (m), 2870 (w), 1578 (m), 1490 (s), 1242 (s), 972 (s), 753 (s).

### 4.4 Liquid–liquid extraction

The organic phase was prepared by dissolving appropriate amounts of CE ($m \approx 3$ mg) in 3 mL dichloromethane (concentration of the CE *c*CE ranging from $6.0 \times 10^{-3}$ to $8.0 \times 10^{-3}$ mol $L^{-1}$). The aqueous phase was prepared by diluting salts in water at CE : salt molar ratio between 25 : 1 to 11 : 1 (concentration of the salts *c*Salt ranging from $2.0 \times 10^{-4}$ to $8.0 \times 10^{-4}$ mol $L^{-1}$). For all extraction experiments, the volume ratio of dichloromethane–water was 1 : 1. The extraction proceeded by vigorously shaking the vial for 45 min at 500 rpm at specific temperatures. Phase separation was guaranteed by waiting 30 min after extraction. The aqueous phase was adequately diluted, and the remaining concentration of the metal ion was measured by a UV-vis spectrometer.

### 4.5 Temperature-dependent liquid–liquid extraction

Temperature-dependent extractions were performed with a constant molar concentration of CE : salt = 14 : 1. The extraction conditions were carried out analogously to the conditions described above, with only the temperature being changed in a range between 10 and 30 °C. For the temperature setting, a cooling and heating thermomixer MKR13 (DITABIS) was used, which has a temperature accuracy of ±0.1 °C. The thermomixer was used for the temperature adjustment. To additionally determine the temperature in the solution, a water sample was placed into the thermomixer in which an additional thermometer permanently measured the temperature.

## Author contributions

I. O. and V. A.: conceptualization. I. O. and F. O.: methodology, investigation, data curation, formal analysis, and validation; V. A.: supervision and resources; I. O.: writing the original draft; I. O and V. A.: review and editing of the original draft.

## Conflicts of interest

There are no conflicts to declare.

## Acknowledgements

The authors acknowledge the NMR spectroscopy and mass spectrometry division of the Department of Chemistry at the Universität Hamburg, and Prof. Dr Weller for providing access to the DSC instrument.

## Notes and references

1 J. C. Shen, W. L. Jiang, W. Di Guo, Q. Y. Qi, D. L. Ma, X. Lou, M. Shen, B. Hu, H. B. Yang and X. Zhao, A rings-in-pores net: Crown ether-based covalent organic frameworks for phase-transfer catalysis, *Chem. Commun.*, 2020, **56**, 595–598.
2 C. J. Pedersen, Cyclic Polyethers and Their Complexes with Metal Salts, *J. Am. Chem. Soc.*, 1967, **89**, 7017–7036.
3 G. W. Gokel, W. M. Leevy and M. E. Weber, Crown ethers: Sensors for ions and molecular scaffolds for materials and biological models, *Chem. Rev.*, 2004, **104**, 2723–2750.
4 A. Boda, S. Musharaf Ali, H. Rao and S. K. Ghosh, Ab initio and density functional theoretical design and screening of model crown ether based ligand (host) for extraction of lithium metal ion (guest): Effect of donor and electronic induction, *J. Mol. Model.*, 2012, **18**, 3507–3522.
5 F. Yan, H. Liu, H. Pei, J. Li, Z. Cui and B. He, Polyvinyl alcohol-*graft*-benzo-15-crown-5 ether for lithium isotopes separation by liquid–solid extraction, *J. Radioanal. Nucl. Chem.*, 2017, **311**, 2061–2068.
6 M. Kamenica, R. R. Kothur, A. Willows, B. A. Patel and P. J. Cragg, Lithium ion sensors, *Sensors*, 2017, **17**, 2430.
7 P. E. Stott, J. S. Bradshaw and W. W. Parish, Modified Crown Ether Catalysts. 3. Structural Parameters Affecting Phase

Transfer Catalysis by Crown Ethers and a Comparison of the Effectiveness of Crown Ethers to That of Other Phase Transfer Catalysts, *J. Am. Chem. Soc.*, 1980, **102**, 4810–4815.

8 S. Tas, B. Zoetebier, M. A. Hempenius, G. J. Vancso and K. Nijmeijer, Monovalent cation selective crown ether containing poly(arylene ether ketone)/SPEEK blend membranes, *RSC Adv.*, 2016, **6**, 55635–55642.

9 A. Casadellà, A. H. Galama, O. Schaetzle and K. Loos, Effect of Diffusion and Migration on the Selectivity of a Polymer Inclusion Membrane Containing Dicyclohexano-18-crown-6, *Macromol. Chem. Phys.*, 2016, **217**, 1600–1606.

10 I. Oral and V. Abetz, A Highly Selective Polymer Material using Benzo-9-Crown-3 for the Extraction of Lithium in Presence of Other Interfering Alkali Metal Ions, *Macromol. Rapid Commun.*, 2021, **42**, 2000746.

11 I. Oral, L. Grossmann, E. Fedorenko, J. Struck and V. Abetz, Synthesis of Poly(methacrylic acid)-*block*-Polystyrene Diblock Copolymers at High Solid Contents via RAFT Emulsion Polymerization, *Polymers*, 2021, **13**, 3675.

12 I. Oral and V. Abetz, Improved alkali metal ion capturing utilizing crown ether-based diblock copolymers in a sandwich-type complexation, *Soft Matter*, 2022, **18**, 934–937.

13 K. Kimura, S. Kanokogi and M. Yokoyama, Extraction Spectrophotometry of Lithium Ions Based on Cation-and Photo-Induced Isomerization of Crowned Spirobenzopyran, *Anal. Sci.*, 1996, **12**, 399–403.

14 Y. Tian, W. Chen, Z. Zhao, L. Xu and B. Tong, Interaction and selectivity of 14-crown-4 derivatives with Li +, Na +, and Mg2+ metal ions, *J. Mol. Model.*, 2020, **26**, 67.

15 K. Sambe, N. Hoshino, T. Takeda, T. Nakamura and T. Akutagawa, Dynamics and Structural Diversity of Li + (Crown Ether) Supramolecular Cations in Electrically Conducting Salts, *J. Phys. Chem. C*, 2020, **124**, 13560–13571.

16 Y. Katayama, K. Nita, M. Ueda, H. Nakamura, M. Takagi and K. Ueno, Synthesis of chromogenic crown ethers and liquid-liquid extraction of alkali metal ions, *Anal. Chim. Acta*, 1985, **173**, 193–209.

17 R. E. C. Torrejos, G. M. Nisola, S. H. Min, J. W. Han, S. Koo, K. J. Parohinog, S. Lee, H. Kim and W. J. Chung, Aqueous Synthesis of 14-15-Membered Crown Ethers with Mixed O, N and S Heteroatoms: Experimental and Theoretical Binding Studies with Platinum-Group Metals, *ChemPlusChem*, 2019, **84**, 210–221.

18 Y. Inoue, T. Hakushi, Y. Liu and L. H. Tong, Molecular Design of Crown Ethers. 12. Complexation Thermodynamics of 12- to 16-Crown-4: Thermodynamic Origin of High Lithium Selectivity of 14-Crown-4, *J. Org. Chem.*, 1993, **58**, 5411–5413.

19 Y. Tobe, Y. Tsuchiya, H. Iketani, K. Naemura, K. Kobiro, M. Kaji, S. Tsuzuki and K. Suzuki, Synthesis and lithium ion selectivity of 14-crown-4 derivatives having bulky subunits: cis and trans isomers of 2-phenylcyclohexano-14-crown-4,2,3-diphenylcyclohexano-14-crown-4 and 2,3-di-(1-adamantyl)-14-crown-4, *J. Chem. Soc., Perkin Trans. 1*, 1998, (3), 485–494.

20 I. Oral, S. Tamm, C. Herrmann and V. Abetz, Lithium Selectivity of Crown Ethers: The Effect of Heteroatoms and Cavity Size, *Sep. Purif. Technol.*, 2022, 121142.

21 A. Warshawsky and N. Kahana, Temperatre-Regulated Release of Alkali Metal Salts from Novel Polymeric Crown Ether Complexes, *J. Am. Chem. Soc.*, 1982, **104**, 2663–2664.

22 G. Martin, L. Rentsch, M. Höck and M. Bertau, Lithium market research – global supply, future demand and price development, *Energy Storage Mater.*, 2017, **6**, 171–179.

23 I. Ore, I. O. Pigments, P. Rock, Q. Crystal, R. Earths and S. Ash, *Mineral Commodity Summaries 2021*, 2021.

24 S. V. Demin, N. A. Shokurova, L. I. Demina, L. G. Kuz'mina, V. I. Zhilov and A. Y. Tsivadze, Effects of Side-Chain Substituents in Benzo-15-Crown-5 on Lithium Extraction, *Russ. J. Inorg. Chem.*, 2018, **63**, 121–127.

25 K. Wilcox and G. E. Pacey, Chromogenic benzo- and monoaza-12-crown-4, 13-crown-4 and 14-crown-4 lithium-selective, *Talanta*, 1991, **38**, 1315–1324.

26 C. Shi, Y. Jia, J. Xiao, X. Wang, Y. Yao and Y. Jing, Lithium isotope separation by liquid-liquid extraction using ionic liquid system containing dibenzo-14-crown-4, *J. Mol. Liq.*, 2016, **224**, 662–667.

27 K. Nishizawa, S. I. Ishino, H. Watanabe and M. Shinagawa, Lithium isotope separation by liquid-liquid extraction using benzo-15-crown-5, *J. Nucl. Sci. Technol.*, 1984, **21**, 694–701.

28 N. Alizadeh, A comparison of complexation of Li+ ion with macrocyclic ligands 15-crown-5 and 12-crown-4 in binary nitromethane-acetonitrile mixtures by using lithium-7 NMR technique and ab initio calculation, *Spectrochim. Acta, Part A*, 2011, **78**, 488–493.

29 A. Pálsdóttir, C. A. Alabi and J. W. Tester, Characterization of 14-Crown-4 Ethers for the Extraction of Lithium from Natural Brines: Synthesis, Solubility Measurements in Supercritical Carbon Dioxide, and Thermodynamic Modeling, *Ind. Eng. Chem. Res.*, 2021, **60**, 7926–7934.

30 Z. Zhang, Y. Jia, B. Liu, H. Sun, Y. Jing, Q. Zhang, F. Shao, M. Qi and Y. Yao, Study on behavior of lithium ion in solvent extraction and isotope separation, *J. Mol. Liq.*, 2021, **324**, 114709.

31 H. Wang, J. He, J. Liu, S. Qi, M. Wu, J. Wen, Y. Chen, Y. Feng and J. Ma, Electrolytes Enriched by Crown Ethers for Lithium Metal Batteries, *Adv. Funct. Mater.*, 2021, **31**, 1–9.

32 Y. Oba, M. Okuhata, T. Osakai and T. Mochida, Solvate and protic ionic liquids from aza-crown ethers: Synthesis, thermal properties, and LCST behavior, *Phys. Chem. Chem. Phys.*, 2018, **20**, 3118–3127.

33 D. Taziaux, J. P. Soumillion and J. L. Habib Jiwan, Photophysical and complexing properties of new fluoroionophores based on coumarin 343 linked to rigidified crown-ethers, *J. Photochem. Photobiol., A*, 2004, **162**, 599–607.

34 S. Obst and H. Bradaczek, Molecular dynamics study of the structure and dynamics of the hydration shell of alkaline and alkaline-earth metal cations, *J. Phys. Chem.*, 1996, **100**, 15677–15687.

35 A. Williamson, XXII. – On Etherification, *J. Chem. Soc.*, 1852, **4**, 229–239.

36 T. Laue and A. Plagens, *Namen- und Schlagwort-Reaktionen der Organischen Chemie*, Teubner, 4th edn, 2004.

37 W. Bin Huang, Y. Guo, J. A. Jiang, X. D. Pan, D. H. Liao and Y. F. Ji, An efficient strategy for protecting dihydroxyl groups of catechols, *Synlett*, 2013, 741–746.

38 J. W. Yuan, H. Y. Qiu, P. F. Wang, J. A. Makawana, Y. A. Yang, F. Zhang, Y. Yin, J. Lin, Z. C. Wang and H. L. Zhu, Synthesis of caffeic acid amides bearing 2,3,4,5-tetrahydrobenzo[ b][1,4]dioxocine moieties and their biological evaluation as antitumor agents, *Molecules*, 2014, **19**, 7269–7286.

39 A. Bey, O. Dreyer and V. Abetz, Thermodynamic analysis of alkali metal complex formation of polymer-bonded crown ether, *Phys. Chem. Chem. Phys.*, 2017, **19**, 15924–15932.

40 P. W. Linder and K. Murray, Correction of formation constants for ionic strength, from only one or two data points: An examination of the use of the extended Debye-Hückel equation, *Talanta*, 1982, **29**, 377–382.

41 G. Donnay and J. W. Gryder, The oxygen coordinations of lithium, *J. Chem. Educ.*, 1965, **42**, 223.

42 C. W. Bock, A. Kaufman and J. P. Glusker, Coordination of Water to Magnesium Cations, *Inorg. Chem.*, 1994, **33**, 419–427.

43 A. F. Holleman and N. E. Wiberg, *Lehrbuch der Anorganischen Chemie*, Gruyter, Walter de, 102nd edn, 2007.

44 R. G. Parr and R. G. Pearson, Absolute Hardness: Companion Parameter to Absolute Electronegativity, *J. Am. Chem. Soc.*, 1983, **105**, 7512–7516.

45 E. C. Koch, Acid-base interactions in energetic materials: I. The Hard and Soft Acids and Bases (HSAB) principle - Insights to reactivity and sensitivity of energetic materials, Propellants, *Explos. Pyrotech.*, 2005, **30**, 5–16.